Extraordinary runoff from the Greenland Ice Sheet in 2012 amplified by hypsometry and depleted firn-retention

A.B. Mikkelsen[1,2], Hubbard, A.L.[3,4], MacFerrin, M.[5], Box, J.E.[6], Doyle, S.H.[4], Fitzpatrick, A.[4], Hasholt, B[1].Bailey, H.[4], Lindbäck, K.[7] and Pettersson, R.[7]

[1]{Department of Geosciences and Natural Resource Management, University of Copenhagen, Denmark}

[2]{Centre for Permafrost (CENPERM), University of Copenhagen, Øster Voldgade 10, Copenhagen, DK-1350, Denmark.}

[3]{Centre for Arctic Gas Hydrate, Environment and Climate, Department of Geology, University of Tromsø, Dramsveien 201, N-9037 Norway.}

[4]{Centre for Glaciology, Department of Geography and Earth Sciences, Aberystwyth University, Aberystwyth, SY23 3DB, UK}

[5]{Cooperative Institute for Research in Environmental Sciences (CIRES), University of Colorado, Boulder, CO, USA}

[6]{Department of Glaciology and Climate, Geological Survey of Denmark and Greenland, Copenhagen, Denmark

[7] Department of Earth Sciences, Villay, 16-752 36 Upsala Universitet, Sweden.

Correspondence to: A.B. Mikkelsen (bechmikkelsen@gmail.com)

Abstract

It has been argued that the infiltration and retention of meltwater within firn across the percolation zone of the Greenland ice sheet has the potential to buffer up to ~3.6 mm of global sea level rise (Harper et al., 2012). Despite evidence confirming active refreezing processes above the equilibrium line, their impact on runoff and proglacial discharge has yet to be assessed. Here we compare meteorological, melt, firn-stratigraphy and discharge data from the extreme 2010 and 2012 summers to determine the relationship between atmospheric forcing and melt runoff at the land-terminating, Kangerlussuaq sector of the Greenland ice sheet which drains into Watson River. The 6.8 km^3 bulk discharge in 2012 exceeded that in 2010 by 28%, despite only a 3% difference in net melt energy between the two years. This large disparity can be explained by a 10% contribution of runoff originating from above the long-term equilibrium line (up to 1850 m a.s.l.) in 2012 caused by diminished firn retention. The 2012 discharge response was compounded by catchment hypsometry - the disproportionate increase in the area contributing to runoff as the melt-level rose into the accumulation area.

Satellite imagery and oblique aerial photographs of an active network of supraglacial rivers extending 140 km from the ice margin confirm meltwater runoff originating well above the equilibrium line. This runoff culminated in three days of record discharge of 3,100 $m^3 s^{-1}$ (0.27 Gt d^{-1}) that peaked on 11 July and washed-out the Watson River bridge. Our findings corroborate meltwater infiltration across the percolation zone though the resulting patterns of refreezing are complex and can lead to spatially extensive, perched superimposed layers within the firn. In 2012, such layers extended to an elevation of at least 1840 m providing an semi-impermiable barrier to further meltwater storage and promoting enhanced runoff that contributed directly to global sea-level rise.

1 Introduction

The Greenland ice sheet is losing mass at 0.7 mm yr^{-1} equivalent of global sea-level rise, the majority of which is attributed to surface ablation that is set to increase under atmospheric warming (Enderlin et al., 2014; Hanna et al., 2013). Although surface melt water production can be readily calculated by regional climate models (e.g. Fettweis et al., 2011) such estimates do not equate directly to sea-level rise, due to the hydrological processes that buffer and store melt on, within and beneath the ice sheet. Of these processes, it is those that determine retention near the ice sheet surface, particularly refreezing across the wet-snow/percolation zone above the equilibrium line altitude (ELA), that appear to have the greatest capacity to offset future sea-level rise (Pfeffer et al., 1991). Within the percolation zone, melt generated at the surface infiltrates and refreezes within the snow-pack, increasing its density, forming firn and thereby retaining potential runoff (Pfeffer et al., 1991; Braithwaite et al., 1994). Harper et al. (2012) analysed a series of cores and ground penetrating radar profiles collected across an 85 km transect above the ELA at ~69.5°N to quantify the water storage capacity of the percolation zone. Their analysis revealed repeated infiltration events in which surface melt penetrated to more than 10 m depth and refroze as superimposed ice layers. Although the resulting patterns of vertical densification were complex, they argue that over a period of decades such infiltration will fill all of the available pore space thereby providing a storage sink of between 322 to 1,289 Gt of melt – equivalent to buffering ~0.9 to ~3.6 mm of global sea level rise.

Below the ELA in spring, melt water is initially stored within the snow-pack but once the pore-space is saturated it runs off the previous summer's ice surface (Irvine-Fynn et al., 2011). This runoff either flows directly into the subglacial environment via supraglacial river networks and moulins or is temporarily stored in supraglacial lakes. Such lakes can individually capture up to 10^7 m^3 (≈0.01 Gt) of water (Box and Ski, 2007) and are estimated to cover up to 3% of the ice sheet ablation area. They hence have the capacity to buffer significant volumes of water on timescales from weeks to months and if they do not drain, then potentially years (e.g. Fitzpatrick et al., 2014; Selmes et al., 2011). Once filled, the lakes contribute directly to proglacial discharge either by over-flowing into downstream moulins or by rapid in situ drainage into the subglacial environment (e.g. Das et al., 2008; Doyle et al., 2013). It has been noted that supraglacial lakes often drain in clusters that may then cause major peaks in proglacial discharge (Doyle et al., 2013; Fitzpatrick et al., 2014). Ice-dammed proglacial lakes also provide a temporary buffer to proglacial discharge and are known to drain suddenly (Carrivick and Quincey, 2014; Mikkelsen et al., 2013).

Quantifying these water storage mechanisms across the ice surface is important since the consequence of enhanced melt on mass balance and sea level contribution depends on the fraction of melt that escapes to the ocean. The elevation of the ice sheet undergoing melt will rise under predicted atmospheric warming, and this could force runoff from well within the ice sheet interior and contribute to enhanced sea level rise (Hanna et al., 2008; Huybrechts et al., 2011; Smith et al., 2015). Expansion of the melt area with warming is further amplified by the ice sheet hypsometry. As the ice surface flattens toward higher elevations, a linear increase in the melt level results in a disproportionate gain in the net surface area exposed to melt conditions. If, however, a significant fraction of that melt is subsequently intercepted and stored by local percolation and refreezing within the snow-pack above the ELA, or otherwise at lower elevations in supra- and pro-glacial lakes, then proglacial discharge and sea-level rise will be buffered on a time-scale of weeks to decades. Although these storage terms have been estimated for the ice sheet (Box and Ski, 2007; Carrivick and Quincey, 2014; Fitzpatrick et al., 2014; Harper et al., 2012; Humphrey et al., 2012), their combined impact on runoff and proglacial discharge in an integrated study has yet to be quantitatively assessed.

In this study, through reference to the two successive extreme-melt seasons of 2010 and 2012, we quantify the efficacy of surface melt storage processes across the Greenland ice sheet using a hydrological-budget approach. We compare surface melt with proglacial discharge across a well-defined, land-terminating catchment that drains the Kangerlussuaq sector of the ice sheet. By drawing on satellite imagery and a series of snow-pits and firn-cores from above the ELA, we then relate the seasonal discrepancies in the hydrological budget to the spatial extent and effectiveness of potential storage terms across the lower accumulation area.

1.1 The exceptional 2010 and 2012 melt-seasons

The record warm Greenland summers of 2010 and 2012 have been studied using regional atmospheric modelling (Tedesco et al., 2013), microclimatological observations (Bennartz et al., 2013; van As et al., 2012), microwave and optical remote sensing (Nghiem et al., 2012; Smith et al., 2015; Tedesco et al., 2011), and in situ data informing an hypsometric analysis (McGrath et al., 2013). In both years, a blocking high pressure, associated with a strongly negative summer North Atlantic Oscillation (NAO) anomaly, was present in the mid-troposphere over Greenland (Hanna et al., 2014). The resulting circulation pattern advected warm southerly winds over the western flank of the ice

sheet, forming an insulating heat-bubble over Greenland (Neff et al., 2014) that promoted enhanced surface heating.

During summer 2010, higher than average near-surface air temperatures in western and south-western regions of the ice sheet led to early and prolonged summer melting and metamorphism of surface snow, significantly reducing surface albedo and thereby enhancing sunlight absorption (van As, 2012; Box et al., 2012; Tedesco et al., 2013). Similarly, in 2012 high near-surface air temperatures and a low surface albedo enabled high melt rates. During 2012 exceptional melt events were concentrated in two periods in mid and late July. On 12 July a ridge of warm air stagnated over Greenland and melt occurred over 98.6% of the entire surface of the ice sheet – even extending to the perennially-frozen, high-elevation interior ice at the ice divide (McGrath et al., 2013; Nghiem et al., 2012). In the Kangerlussuaq sector, the focus of this study, the 11 July 2012 melt-event had a severe and direct hazardous impact with the wash-out and partial destruction of the Watson River bridge on the 11 July 2012 (https://youtu.be/RauzduvIYog), implying that proglacial discharge was at its highest stage since the early 1950's when the bridge was constructed. A second phase of exceptional conditions returned in late July 2012 when 79.2% of the ice sheet surface was again exposed to exceptional melt (Nghiem et al., 2012). Bennartz et al. (2013) found that low-level clouds played an important role by increasing near-surface air temperatures via their effect on radiative absorption. Such clouds were low enough to enhance the downward infrared irradiance whilst being optically thin enough to allow solar radiation to penetrate.

These conditions had the capacity to force rapid and extreme ice sheet melt and runoff that was visible from space and in time-lapse camera sequences of, for example, proglacial flooding (Smith et al., 2015) and turbulent plumes active at the fronts of tidewater glaciers (Chauché et al., 2014; Nick et al., 2012). Nevertheless, the challenge of estimating discharge at marine-terminating glaciers, and the lack of proglacial gauging measurements in Greenland, means that this inference can only be assessed on broad, regional scales using satellite-derived estimates of mass change (e.g. GRACE; Ewert et al., 2012). Hence, these two years of exceptional atmospheric forcing provide an ideal natural experiment and case-study to assess and quantify the catchment-wide efficacy and spatio-temporal footprint of melt, storage and runoff processes across the ice sheet.

2 Study area & methods

2.1 Study area

We focus on the ~ 12,500 km^2 hydrological catchment that drains into Watson River from the land-terminating Kangerlussuaq sector on the western margin of the ice sheet. The catchment is 95% glaciated and comprises four main outlet glaciers centred on Russell Glacier (Figure 1). Within this catchment, the ice surface rises ~90 km from the ice margin at 550 m a.s.l. to the mean (1990 - 2010) ELA of 1,553 m a.s.l.(van de Wal et al., 2012; 2015), and extends a further ~150 km across the accumulation area to the ice divide at ~2,550 m a.s.l.

2.2 Proglacial discharge measurements

Proglacial river discharge was gauged near the Watson River bridge in Kangerlussuaq, located 22km from the ice sheet margin. Due to orographic shielding by Sukkertoppen Ice Cap (Box et al., 2004; van den Broeke et al., 2008) the Kangerlussuaq region is exceptionally dry, with a mean annual precipitation of 149 mm. Land surface water losses from evaporation and sublimation further minimise the land area contribution to runoff compared to the ice sheet component (Hasholt et al., 2013). Watson River discharge was determined using the stage/discharge relationship presented in Hasholt et al. (2013). Water stage was recorded by pressure transducers on a stable cross section ~100 m upstream from the bridge. The discharge Q is given by

$$Q = V \times A, \qquad \text{Eq. 1}$$

where V represents the mean velocity in the river cross-section and A is the cross-sectional area. The surface velocity (V) was measured by means of a float and converted into mean cross-sectional velocity by applying a reduction factor of 0.95 (Hasholt et al., 2013). The cross-sectional area (A) used for discharge calculations is based on the deepest sounding of the channel bottom after the winter ice melts in spring. The combined uncertainty in the cross-sectional area and velocity measurements is estimated to be 15% (Hasholt et al., 2013). However, here we also conservatively include the possibility of a systematically deeper cross section due to bed erosion within the deepest of the two channels during the runoff season. Therefore we estimate the upper limit in the yearly cumulative discharge for 2010 and 2012 at +44% and +32% respectively. The instantaneous possible error varies with the discharge rate, and is plotted together with the measured discharge (Figure 2D and E).

During the flood event on 11 July 2012 the water level exceeded the previously observed maximum water stage by 1.65 m (15%) and the stage-discharge relationship was extrapolated accordingly. Our stage-discharge relationship was also altered by the partial removal of a road dam (part of the bridge construction), which opened up two new, shallow channels between and south of the two original channels (Figure 3). We measured the cross-sectional area of the two new channels after the flood had subsided, and by combining these measurements with estimates of the stage from time-stamped time-lapse photograph, we estimate that these new channels were 1.5 and 2.5 m deep at peak flow.

The surface velocity in these new channels was calculated assuming the conservation of energy in fluids:

$$v = \sqrt{2gh} \qquad \text{Eq. 2}$$

where v is the surface velocity of the water, g is the gravitational acceleration (9.82 m/s^2) and h is the water level. The uncertainty in v for the two new channels is predominantly attributed to the determination of stage from time-lapse photos which we conservatively estimate at ~30%. The two original bedrock channels remained intact and we assume that the hydraulic conditions in these channels did not change substantially during the flood event. For the period after the bridge foundation was partially washed out, the amount of discharge in the new channels is added to that calculated based on the stage/discharge relationship for the original channels. We estimate that the formation of the two new channels during the flood event resulted in a low relative (i.e. < 3%) contribution to the total discharge and they therefore do not substantially alter our results.

2.3 Meteorological measurements

Automatic weather stations (AWS) are located at three elevations: 732 m a.s.l. (AWS_L), 1280 m a.s.l. (AWS_M) and 1840 m a.s.l. (AWS_U) (see van As et al., 2012). Each AWS, recorded near-surface (2-3m) air temperature, humidity, wind speed, upward and downward shortwave and long wave irradiance, and air pressure.

2.4 Snow and ice albedo

Surface albedo was determined from NASA's Terra Satellite's Moderate Resolution Imaging Spectroradiometer (MODIS) interpolated onto a 5 km grid from 1 May 2010 to 31 September, 2012.

187 An 11-day running median was taken to reject noise caused by contrails and cloud shadows (Box et
188 al., 2012). From these data an albedo time series was formed for the glaciated part of the Watson
189 River catchment area defined as 67±0.2 °N, and west of 44°W. The data were averaged in 100 m
190 elevation intervals. The resulting albedo product was divided into three approximately equal-area
191 bands corresponding to the physiographic regions dominated by surface impurity darkness (1000 to
192 1450 m a.s.l.), lakes (1500 – 1650 m a.s.l.) and wet-snow (1700 – 1850 m a.s.l.) (Figure 1) (see also
193 Wientjes et al., 2012; Wientjes and Oerlemans, 2010).

194 2.5 Surface energy budget model

195 The surface energy budget (SEB) was calculated daily across the glacierized catchment following
196 van As et al. (2012). The model calculates radiative, turbulent, rain and subsurface (conductive)
197 energy fluxes using data from the three AWS measurements as input, interpolated into the same 100
198 m elevation bins as the albedo data. The MODIS albedo data were used in the calculation of net
199 shortwave radiation. The sensible and latent energy fluxes were calculated from near surface
200 gradients of wind speed, temperature and humidity using a stability correction. The surface mass
201 balance (SMB) is calculated as the sum of solid precipitation, surface melt and sublimation. The
202 model was validated against independent K-transect measurements (e.g. van de Wal et al., 2012) and
203 its performance was found to be within 4% of the observed values. The net energy available for melt
204 across the entire glacierized-catchment was determined by integrating the calculated energy flux (W
205 m^{-2}) for each elevation interval by area. For the purpose of quantifying the potential net melt available
206 for runoff, refreezing and retention parameterisations were disabled.

207 2.6 Firn Saturation Model

208 Based upon firn core stratigraphy and density measurements at AWS_U, a simple model was
209 produced to illustrate when horizontal water flow might occur if melt water were not permitted to
210 percolate beneath the massive 2010 ice layers. Water generated by melt at the surface, minus
211 evaporation/sublimation, fills the available pore-space of the firn beneath and raises the saturated
212 water table level. In situ measurements and/or reasonable ranges were assigned for model input
213 values, including the density of fresh snow, the average depth and density of the packed snow layer
214 above the firn, the density of refrozen ice and the amount of water attributed to sublimation and
215 evaporation. Ten million (107) Monte Carlo model iterations were run over the range of input

variables to produce 95% confidence intervals of the daily water levels and potential firn saturation dates at KAN_U.

2.7 Supraglacial lake drainage

To determine the extent and timing of supraglacial lake drainage events within the Watson River catchment, an automatic lake classification was applied to daily MODIS MOD09 imagery following Fitzpatrick et al. (2014). Fifty-two cloud-free images were processed to derive the surface area and volume of supraglacial lakes. Lake areas are classified using an empirically-determined threshold of the Normalised Difference Water Index (NDWI; Huggell et al., 2002). Lake volume is derived using a reflective index approach after Box and Ski (2007) calibrated against lake bathymetry data that was acquired in 2010 (Doyle et al., 2013), and subsequently validated against in-situ depths from an independent supraglacial lake at 67° N, 48°W, at ~1420 m.a.s.l. (Fitzpatrick et al., 2014). The error in our lake area and depth are estimated at ±0.2 km^2 per lake and 1.5 m per pixel respectively. Change in stored volume in each lake was converted to mean discharge rates between cloud-free observations (Figure 2 D&E).

2.8 Catchment delineation

A well documented source of uncertainty in calculating runoff stems from the delineation of hydrologically complex watersheds characterised by rapidly evolving supraglacial stream, river and lake networks (e.g. van As et al., 2012; Fitzpatrick et al., 2014; Smith et al., 2015). Furthermore, the supraglacial drainge system is only part of the water-transport story and subsequent routing of meltwater on injection into the basal environment via moulins and fractures remains poorly accounted. Here we adopt a novel watershed deline ation approach based on the subglacial catchment and drainge routing determined from hydropotential analysis (see Lindbäck et al., 2015). In their analysis, Lindbäck et al. (2015) demonstrate that the spatial extent and footprint of the Watson River catchment evolved by up to 30% according to variable subglacial hydrological and water-pressure conditions over the course of the melt-season. However, they also note that despite significant hydrological piracy between adjacent catchments, the actual contributing area of the Watson River subglacial catchment, along with its hypsometry, remains effectively constant. Moreover, Lindback et al. (2015) also demonstrate that across the lower ablation area (500 to 1250

m asl.) where melt-rates are highest, this assumption holds even under transient water-pressure conditions. We are thus confident that our catchment deliniation based on a steady-state subglacial hydropotential anaysis and the resulting runoff estimates are robust given available data-sets.

2.9 Measurements of firn and snow pack density

To assess firn and snow-pack densification, 15 snow-pits and three 7.6-cm-diameter ice cores were obtained from eight sites between 1280 and 1840 m a.s.l. in April 2012. Two cores (#1 and #2) were drilled 10 m apart in the direct vicinity of AWS_U while core #3 was drilled at a site located 400 m to the south of AWS_U. The core stratigraphy was analysed at ~1 cm vertical resolution before cores were cut into 10 cm sections and weighed to determine the density profile of the snowpack and firn. A transect of 0.5 to 1 m-deep snow-pits between AWS_M and AWS_U were examined to investigate spatial variations in firn and snowpack density (Figure 1).

3 Results

Near-surface air temperatures from three AWS reveal insightful differences in the temporal and altitudinal distribution of melt energy between 2010 and 2012. Melt commenced earlier in 2010 with the lowest AWS_L reaching 6°C daily average air temperature by mid-May (Figure 2A). At AWS_L, melt with air temperature 5°C above the seasonal average persisted until 15 September. The duration of the 2010 melt-season (119 days) was without precedent for the Kangerlussuaq sector of the ice sheet since 1973 (van As et al., 2012). At the uppermost AWS_U, located ~300 m above the 1991-2009 baseline ELA of 1524 m (van de Wal et al., 2012), above-freezing temperatures did not prevail until 8 July, 2010. Thereafter daily temperatures remained above melting until September making 2010 exceptional for melt compared to the long-term average.

During the 2012 melt season, air temperatures at elevations above the mean ELA indicated surface melt mid-June onwards and included two week-long periods with extreme daily air temperatures at AWS_U of 3 to 4°C (Figure 2A), coinciding with high barometric pressure and associated clear sky conditions. During the 5-days leading up to the extreme mid-July 2012 melt event, air temperatures at AWS_M and AWS_U were within 1°C despite being separated by 70 km and having 500 m elevation separation. Hence, from mid June and throughout July 2012, the environmental lapse rate was exceptionally low – indicating that melting conditions prevailed across the relatively flat lower

accumulation area. By the 12 July, melt extended to the topographic peak of the ice sheet (McGrath et al., 2013; Nghiem et al., 2012). Below 1000 m a.s.l., the mean 2012 summer air temperatures were in contrast 0.75°C lower than in 2010, though still higher than the long-term mean. This is partly explained by the delayed 2012 melt onset, commencing in late May 2012 (Figure 2A).

The net cumulative energy available for surface melt across the glacierized-portion of the catchment are virtually equivalent by the end of 2010 and 2012 melt-seasons despite contrasting melt season development (Figure 2B). The total energy available for melt in 2010 and 2012 calculated using the SEB model for the catchment up to an elevation of 1840 m a.s.l was just 3% less in 2012, compared to 2010 (Table 1).

MODIS albedo time-series (Figure 2C) binned into three elevation bands equating to the extent of the dark-, lake- and wet-snow zones, respectively (Figure 1) exhibit complex patterns of change through space and time. In 2012, the albedo decline lags behind 2010 (Figure 2C) due to the early-May melt onset in 2010 promoted by low 2009/2010 winter snow accumulation (van As et al., 2012). By mid-June, albedo across the dark zone for both years declined to 0.4. For the remainder of the melt season, the 2010 dark zone albedo was ~0.05 lower than in 2012 (Figure 2C), consistent with warmer temperatures and enhanced melt at low elevations during the 2010 melt season. Across the lake and wet-snow zones, a similar pattern of albedo decline is observed up until mid-June. From this time onward, in contrast to the dark zone, it is 2012 albedo that is consistently and as much as 0.2 lower than 2010, with the exception of a week-long, snow-fall albedo reset on 5 August 2012. Enhanced black carbon deposition from North American wildfire may have played a key role in driving the exceptionally low albedo at high elevations in 2012 (Keegan et al., 2014).

The seasonal evolution of daily Watson River discharge and catchment-integrated melt vary considerably between 2010 and 2012 (Figure 2D to F). In 2010 the integrated melt and discharge increased at a slower rate than in 2012, despite higher cumulative energyinput aided by high temperatures and and lower albedo. 2012 integrated discharge peaked at 3100 m^3 s^{-1} (equivalent to ~0.27 km^3 d^{-1}; Figure 4E) in mid-July, and which washed-out Watson River bridge. With lower temperatures during the week commencing the 15 July, melt and discharge dropped to below 2010 levels but returned to high values (~1500 m^3 s^{-1}) for 11 days starting on 26 July, coincident with the second phase of exceptionally warm conditions. The annual total discharge in 2012 of 6.8 km^3 -15/+32% exceeded the 2010 total of 5.3 km^3 by ~28%.

304 Throughout the 2010 melt-season, a steady increase in the residual between calculated melt across
305 the catchment and cumulative proglacial discharge is apparent which by the end of the season equates
306 to 33% (~1.8 km^3) of residual melt retained (R') within the catchment (Figure 2F) compared to the
307 measured discharge. In the period leading up to 11 July, 2012 a similar R' as compared to 2010
308 suggests meltwater storage. After 11 July 2012 however, R' drops by 40% from more than 1 km^3
309 within 5 days and reduces further by the end of the season indicating that ~ 0.2 km^3 of meltwater is
310 retained in the catchment, and that meltwater retention after 11 July 2012 was limited. The plot of
311 cumulative energy input versus cumulative discharge in 2010 and 2012 (Figure 4) demonstrates a
312 contrasting catchment response to varying surface energy budget between the two years. The slope
313 of the cumulative measured discharge versus cumulative calculated energy input is steeper in 2012
314 than in 2010. Hence, for a given energy input, there was a higher Watson river discharge response in
315 2012 compared to 2010 particularly during the 11 to 14 July 2012 melt-event when the discharge
316 response to the energy input is even stronger.

317 Table 2 lists calculated melt totals from different elevation bands with bulk Watson River
318 discharge and their differences. Below the mean ELA, 2010 and 2012 have roughly equivalent (7%
319 difference) calculated melt. By contrast, above the ELA at elevations up to 1850 m and 2050 m a.s.l.,
320 the calculated melt was 97 and 232 % larger in 2012 compared to 2010 for the elevations 1550 to
321 1850 and 1850 to 2050 respectively (only melt up to 1850 m. asl. is included in Figure 2F and 3).
322 Despite this, the difference in total calculated melt between the two years, was still within 2%,
323 depending on the elevation band to which melt is included. Yet, the difference in measured proglacial
324 discharge between the two years peaks at 28%. Thus, the runoff response to surface energy input was
325 significantly higher in 2012, reflected in the larger residual between calculated melt and measured
326 proglacial discharge (Figure 2F) and further illustrated by the contrasting discharge response to
327 energy flux compared to 2010 (Figure 4).

328 The timing of catchment-integrated melt and Watson River discharge (Figure 2D and E)
329 demonstrates that meltwater routing through the glacial and proglacial system has a lag of between 1
330 to 5 days over each melt-season. In June 2012, the proglacial discharge response to melt was
331 dampened and delayed. Prior to the 11 July 2012 extreme melt and discharge, the integrated modelled
332 melt closely resembles the proglacial discharge hydrograph but with a ~3 day lag. Henceforth through
333 July and the beginning of August 2012, the discharge responds to melt production with a shorter lag.
334 The implication is that once local meltwater production had been mobilised, even at high elevations

335 above the ELA, the runoff transits within 3 days through a drainage network up to 160 km distant
336 from the gauging station, eventually contributing to the proglacial discharge peak. Such a drainage
337 system with supra- and sub-glacial mean transit velocities >2 km h^{-1} (~0.6 m s^{-1}) may be considered
338 efficient on comparison to similar transit velocities derived from tracer-experiments conducted up to
339 57 km from the ice margin in 2011 (Chandler et al., 2013). The second phase of intense melt,
340 commencing on 26 July 2012 resulted in a rapid rise in discharge with a lag of just 2 days. Peak melt
341 during this period occurred on 3 August with the peak in proglacial discharge occurring two days
342 later. The onset of discharge abatement is concurrent with declining air temperatures from 6 August
343 2012 onwards.

344 The release of water stored in supraglacial lakes accounts for a very minor component of
345 proglacial discharge. In 2012 the majority of lake drainages occurred well before any peaks in
346 proglacial discharge (Figure 2E and F). The calculated mean drainage rate of <100 m^3 s^{-1} for 2012
347 clearly indicates that the volume of lake drainage water contributed less than 2% of the total bulk
348 discharge (Figure 2 D&E). The maximum short-term contribution from lake drainage (0.10 km^3)
349 occurred on 23 June 2012 with the concurrent drainage of a cluster of five lakes (Figure 2E). Over
350 the following week, approximately 70% of all the water stored in supraglacial lakes across the
351 catchment was released (Figure 2E), which could have potentially accounted for as much as half of
352 the Watson River discharge. However, this synchronous/multiple lake drainage event occurred ~12
353 days before the proglacial discharge peak of 11 July 2012. Supraglacial lakes can empty in as little
354 as 2 hours (Das et al., 2008; Doyle et al., 2013) and it is very likely that this water stored in
355 supraglacial lakes exited the catchment well before 11 July. One ~0.02 km^3 lake drainage event
356 between 5 and 8 July would likely to have contributed some ~2% to the extraordinary discharge
357 measured between July 10 and 14 (0.9 km^3).

358 MODIS and Landsat imagery reveal that no proglacial ice-dammed lakes within the catchment
359 drained prior to the flooding event, including a number that appear to drain regularly in
360 August/September each year (Mikkelsen et al., 2013). On 11 September 2010 and 12 August 2012, a
361 couple of proglacial lakes did drain, and even though they are evident in the Watson River
362 hydrography, their net contribution to the proglacial discharge is minor (Figure 2D and E).

363

4 Discussion

Our observations that the net atmospheric forcing represented by the incoming energy flux for 2010 and 2012 was equivalent (Figure 4) yet the ensuing runoff response was markedly different. Widespread melt in 2010 has been ascribed to atmospherically-sourced heating coupled with the albedo feedback promoted by low winter snowfall and early melt onset (Tedesco et al., 2011; Box et al., 2012; van As et al., 2012). Yet low albedo and high air temperatures alone cannot explain the 28% increase in discharge in 2012 compared to 2010. MODIS analysis confirms that the release of stored water from supraglacial lakes played a relatively minor role in the peak and total proglacial hydrograph in 2012 (Fig 2D and E). At most, the supraglacial lake contribution to the 11 July 2012 peak discharge of 3,100 m s^{-1} was ~2%. Our results indicate that only a relatively small proportion of the total melt generated at the surface is stored in supra- and pro-glacial lakes and that the buffering effect of lakes on runoff and discharge is therefore limited (Figure 2D and E). That is not to dismiss the role of supraglacial lakes in ice sheet hydrology, since it is the ephemeral storage of surface meltwater in them that enable the critical volume required to initiate and propagate new hydrofractures and moulins to the bed (Krawczynski et al., 2009). In this manner, supraglacial lakes are key to creating efficient englacial pathways for discharging surface water into the subglacial environment over the melt-season (Das et al., 2008; Doyle et al., 2013).

We infer three mutually compatible explanations for the exceptional discharge response observed in 2012: 1) that significant melt occurred above as well as below the ELA, 2) that ice surface hypsometry amplified the melt originating from the accumulation zone by disproportionately increasing the contributing area when melt-levels rose above the ELA, and, 3) there was reduced firn-retention and storage capacity within the accumulation zone that promoted large scale runoff. It is significant that such a large runoff contribution from the percolation zone could only have been attained if firn-retention capacity was severely reduced in 2012 and it is this hypothesis that herein forms the central tenet of our discussion. In support of this we present three additional lines of evidence: A) snow pit observations and ice core stratigraphy acquired in April 2012, B) observations of surface water networks obtained from satellite imagery and oblique photographs from the vicinity of AWS_U (Figure 6), and, C) results of our SEB-modelling experiments where total integrated melt is assumed to runoff without any retention or refreezing.

Our core stratigraphic analysis (Figure 5A to C) reveals significant perched superimposed ice layers that could be capable of blocking surface meltwater infiltration into deeper unsaturated firn

395 layers across the percolation zone. In addition to the shallow ice cores presented (Figure 5), a
396 persistent and continuous decimetre-thick layer of refrozen, superimposed ice was also observed in
397 15 snow pits dug along a transect from extending from below the ELA (1500 m a.s.l.) to AWS_U
398 (Figure 1). Severely reduced firn-retention due to such a superimposed, perched ice lens is further
399 supported by energy balance modelling of the near-surface water table at AWS_U (Figure 5D). Here
400 two potential sets of blocking-layers at different levels within the snow-pack equate to the thick
401 superimposed ice lenses observed in the firn cores acquired at AWS_U (Figure 5A to C). For the
402 shallowest of these scenarios, melt and retention calculations predict complete saturation and free
403 surface water available for active runoff by 11 July 2012. Our results are consistent with a recent
404 study by Machguth et al. (2015) who also demonstrate reduced meltwater retention across the
405 percolation zone of western sector of the Greenland ice sheet.

406 Evidence for firn saturation and active surface runoff are furnished independently by the
407 identification of an active supraglacial channel network in Landsat satellite imagery and from oblique
408 photographs taken 13 August 2012 in the vicinity of AWS_U (Figure 6). In the Landsat imagery, wet
409 snow, meltwater channels and lakes can be identified up to at least 1750 m a.s.l. on 23 June 2012,
410 and an active stream network up to 1840 m a.s.l. from 5 July 2012 onwards. In early August, 2012 an
411 active channel network was confirmed during a scheduled maintenance visit to AWS_U (Figure 6B
412 and C). The supraglacial hydrological network that is evident above the long-term ELA in the period
413 leading up to the 2012 peak discharge event confirms the snow-pack modelling presented. The
414 oblique aerial photos provide unequivocal evidence for surface runoff from this region.

415 MODIS analysis confirms that the release of stored water from supraglacial lakes played a
416 relatively minor role in the peak and total proglacial hydrograph in 2012 (Fig 2D and E). At most,
417 change in supraglacial lake storage contributed just 2 % to the 11 July 2012 peak discharge of 3,100
418 m s^{-1} was ~2%. Our results indicate that only a relatively small proportion of the total melt generated
419 at the surface is stored in supra- and pro-glacial lakes and that the buffering effect of lakes on runoff
420 and discharge is therefore limited (Figure 2D and E). That is not to dismiss the importance of
421 supraglacial lakes in ice sheet hydrology, since it is the ephemeral storage of surface meltwater in
422 them that enable the critical volume required to initiate and propagate new hydrofractures and
423 moulins to the bed (Krawczynski et al., 2009). In this manner, supraglacial lakes are key to creating
424 efficient englacial pathways for discharging surface water into the subglacial environment over the
425 melt-season (Das et al., 2008; Doyle et al., 2013).

If forecast future atmospheric warming is realised, then the combined impact of reduced firn retention capacity and ice sheet hypsometry will become increasingly apparent through amplification of runoff and discharge response with interior melting. If, as we hypothesise, the extraordinary 2012 discharge was substantially derived from runoff originating above the ELA due to an impermeable, superimposed ice lens that formed during previous warm summers, then the 2012 record-warm event itself will drive the formation of even thicker, superimposed ice layers extending yet further into the interior (i.e. McGrath et al., 2013). Hence, we infer a strong positive feedback where a disproportionate and amplified runoff response to future melt events leads to yet more abrupt and severe proglacial discharge as the 11 July 2012 flooding documented here. In light of these findings, the firn-buffering mechanism proposed for the EGIG line some 120 km north of our study area and extrapolated across the entire ice sheet by Harper et al. (2012) would appear to be somewhat diminished, at least in the Kangerlussuaq sector. Based on their data and analysis (Figure 2B and 3C in Harper et al., 2012) and assuming an equivalent location, our AWS_U site, located 50 km beyond, and 300 m above the ELA, should have had a buffering capacity equating to a fill-depth of between 2 m and 10 m of water equivalent melt. In July 2012 at AWS_U this was not the case and under saturated conditions, melt was forced to runoff from the percolation zone into an active supraglacial hydrological network thereby directly contributing to proglacial discharge and sea-level rise.

A key implication of our study is that expected climate warming will change the limit of upper elevation ice sheet runoff to a higher level sooner. The hypsometric effect that amplifies runoff by the contributing area increasing exponentially with elevation (Figure 1) combined with efficient drainage (2-3 day transit times for water (results here and Smith et al. 2015), we may thus expect the ice sheet sea level contribution to be faster than inferred by Harper et al. (2012).

5 Conclusions

Comparison of melt and discharge across the Kangerlussuaq sector in 2010 and 2012 has enabled us to assess, resolve, and attribute the contrasting runoff response of the Greenland Ice Sheet to extreme atmospheric forcing. The bulk discharge of 6.8 km^3 measured in Watson River in 2012 was unprecedented since the Kangerlussuaq bridge was constructed in the early 1950's and exceeded the previous record set in 2010 by ~28%. Throughout the 2010 melt-season, there was a steady increase in the residual between calculated melt across the catchment and cumulative proglacial discharge, which by the end of the season equated to 33% (~1.8 km^3) melt retained within the catchment up to an elevation of 1850 m a.s.l. In the period leading up to 11 July 2012 a similar pattern of storage

457 indicates significant meltwater retention. However, after the 11 July flooding the residual fell by
458 40% and reduced further by the end of September with only 3% (~0.2 km^3) of generated melt retained.
459 The abrupt change signifies a sudden decrease in retention associated with essentially complete
460 surface snow ablation below areas with snow that became water saturated. Surface melt energy versus
461 proglacial discharge demonstrates an amplified response to melt energy in 2012 as compared to 2010,
462 particularly after the 11 July flooding. In 2010 local melting from above the ELA infiltrated, and was
463 stored within the firn as superimposed ice and hence did not contribute to river discharge. In 2012
464 though, our observations and modelling indicate severely reduced firn-layer infiltration and retention
465 due an extensive perched, thick and low permeable ice lens which most likely formed in previous,
466 warm melt years (e.g. 2007 and including 2010).

467 The next decade will reveal if 2010 and 2012 were exceptional melt seasons or are part of an
468 emerging new trend. The three years subsequent to the 2010 and 2012 melt and runoff extremes, i.e.,
469 2013-2015 were marked by low total melt and in some cases anomalously high accumulation. The
470 effect will have been to recharge the buffering capacity of the lower accumulation area to some
471 degree. Either way, it is critical to understand the ice sheet runoff response to such events to determine
472 what portion of the melt generated is intercepted and stored and what fraction directly contributes to
473 proglacial discharge and sea-level rise. Our results reveal that the firn-retention and buffering effects
474 that are argued to dominate the percolation zone were much reduced across the Kangerlussuaq-sector
475 in 2012, and that there was a near-instantaneous discharge response with a disproportionately greater
476 area of the ice sheet above the ELA contributing to runoff and thereby contributing directly to global
477 sea level rise.

478 Acknowledgements

479 We thank Dirk van As and Horst Machguth for assistance in the field and during preparations of the
480 manuscript. We thank Dirk van As for weather station data, runoff calculations, initiating firn
481 investigations, fieldwork logistics, writing and supervisionof Andreas Mikkelsen's PhD project.
482 Gratitude also goes to Paul Smeets, Institute for Marine and Atmospheric Research, Utrecht
483 University for providing oblique areal pictures taken at AWS_U on 13 August 2011. We acknowledge
484 financial support from the Greenland Analogue Project (GAP) – Sub Project A for funding AWS_U
485 and field logistics, the commission on scientific investigations in Greenland, grant no. 07-015998,
486 09-064628 and 2138-08-0003 and the Danish National Research Foundation founding Centre for

Permafrost (CENPERM), funded by the Danish National Research Foundation, DNRF number 100, Department of Geosciences and Nature Resource Management, University of Copenhagen, Denmark for financial support of the discharge measurements. The on-ice weather station in this study was maintained by GEUS and Aberystwyth University. J. Box is here supported by Denmark's "Det Frie Forskningsråd", Nature og Universe grant DFF – 4002-00234. The National Aeronautics and Space Administration (NASA) award NNX10AR76G provided funding for firn table modelling work through the Cooperative Institute for Research in Environmental Sciences, University of Colorado at Boulder, USA. AF and SD were supported by NERC and Aberystwyth University doctoral scholarships respectively and fieldwork was supported by NERC Projects NE/G005796/1, NE/G010595/1, NE/H024204/1 and a Royal Geographical Society Gilchrist Fieldwork Award. A.H. kindly acknowledges support from the Centre for Arctic Gas Hydrate, Environment and Climate by funding from the Research Council of Norway (Grant No. 223259).

499 References

500 Bennartz, R., Shupe, M. D., Turner, D. D., Walden, V. P., Steffen, K., Cox, C. J., Kulie, M. S., Miller,
501 N. B. & Pettersen, C. (2013). July 2012 Greenland melt extent enhanced by low-level liquid
502 clouds. *Nature,* **496**, 83-86.

503 Box, J. E., Bromwich, D. H. & Bai, L.-S. (2004). Greenland ice sheet surface mass balance 1991–
504 2000: Application of Polar MM5 mesoscale model and in situ data. *Journal of Geophysical*
505 *Research,* **109**.

506 Box, J. E., Fettweis, X., Stroeve, J. C., Tedesco, M., Hall, D. K. & Steffen, K. (2012). Greenland ice
507 sheet albedo feedback: thermodynamics and atmospheric drivers. *The Cryosphere,* **6**, 821-
508 839.

509 Box, J. E. & Ski, K. (2007). Remote sounding of Greenland supraglacial melt lakes: implications for
510 subglacial hydraulics. *Journal of Glaciology,* **53**, 257-265.

511 Braithwaite, R. J., Laternser, M. & Pfeffer, T. (1994). Variations of near-surface firn density in the
512 lower accumulation area of the Greenland ice sheet, Pakitsoq, West Greenland. *Journal of*
513 *Glaciology,* **40**, 477-485.

514 Carrivick, J. L. & Quincey, D. J. (2014). Progressive increase in number and volume of ice-marginal
515 lakes on the western margin of the Greenland Ice Sheet. *Global and Planetary Change,* **116**,
516 156-163.

517 Chandler, D. M., Wadham, J. L., Lis, G. P., Cowton, T., Sole, A., Bartholomew, I., Telling, J.,
518 Nienow, P., Bagshaw, E. B., Mair, D., Vinen, S. & Hubbard, A. (2013). Evolution of the
519 subglacial drainage system beneath the Greenland Ice Sheet revealed by tracers. *Nature*
520 *Geoscience,* **6**, 195-198.

521 Chauché, N., Hubbard, A., Gascard, J. C., Box, J. E., Bates, R., Koppes, M., Sole, A., Christoffersen,
522 P. & Patton, H. (2014). Ice–ocean interaction and calving front morphology at two west
523 Greenland tidewater outlet glaciers. *The Cryosphere,* **8**, 1457-1468.Das, S. B., Joughin, I.,
524 Behn, M. D., Howat, I. M., King, M. A., Lizarralde, D. & Bhatia, M. P. (2008). Fracture
525 propagation to the base of the Greenland Ice Sheet during supraglacial lake drainage. *Science,*
526 **320**, 778-781.

527 Doyle, S. H., Hubbard, A. L., Dow, C. F., Jones, G. A., Fitzpatrick, A., Gusmeroli, A., Kulessa, B.,
528 Lindback, K., Pettersson, R. & Box, J. E. (2013). Ice tectonic deformation during the rapid in
529 situ drainage of a supraglacial lake on the Greenland Ice Sheet. *The Cryosphere,* **7**, 129-140.

530 Doyle, S. H., Hubbard, A. et al. (2015), Amplified melt and flow of the Greenland ice sheet driven
531 by late-summer cyclonic rainfall, Nat. Geosci., doi:10.1038/ngeo2482.

532 Enderlin, E. M., Howat, I. M., Jeong, S., Noh, M. J., van Angelen, J. H. & van den Broeke, M. R.
533 (2014). An improved mass budget for the Greenland ice sheet. *Geophysical Research Letters,*
534 **41**, 866-872.

535 Ewert, H., Groh, A. & Dietrich, R. (2012). Volume and mass changes of the Greenland ice sheet
536 inferred from ICESat and GRACE. *Journal of Geodynamics,* **59–60**, 111-123.

537 Fettweis, X., Belleflamme, A., Erpicum, M., Franco, B. & Nicolay, S. (2011). Estimation of the sea
538 level rise by 2100 resulting from changes in the surface mass balance of the Greenland Ice

539 Sheet. *In:* Blanco, J. & Kheradmand, H. (eds.) *Climate Change: Geophysical Foundations*
540 *and Ecological Effects.* Croatia: InTech.

541 Fitzpatrick, A. A. W., Hubbard, A. L., Box, J. E., Quincey, D. J., van As, D., Mikkelsen, A. P. B.,
542 Doyle, S. H., Dow, C. F., Hasholt, B. & Jones, G. A. (2014). A decade (2002 - 2012) of
543 supraglacial lake volume estimates across Russell Glacier, West Greenland. *The Cryosphere,*
544 **8**, 107-121.

545 Hanna, E., Fettweis, X., Mernild, S. H., Cappelen, J., Ribergaard, M. H., Shuman, C. A., Steffen, K.,
546 Wood, L. & Mote, T. L. (2014). Atmospheric and oceanic climate forcing of the exceptional
547 Greenland ice sheet surface melt in summer 2012. *International Journal of Climatology,* **34**
548 **%6**, 1022-1037 %&.

549 Hanna, E., Huybrechts, P., Steffen, K., Cappelen, J., Huff, R., Shuman, C., Irvine-Fynn, T., Wise, S.
550 & Griffiths, M. (2008). Increased Runoff from Melt from the Greenland Ice Sheet: A
551 Response to Global Warming. *Journal of Climate,* **21**, 331-341.

552 Hanna, E., Navarro, F. J., Pattyn, F., Domingues, C. M., Fettweis, X., Ivins, E. R., Nicholls, R. J.,
553 Ritz, C., Smith, B. & Tulaczyk, S. (2013). Ice-sheet mass balance and climate change. *Nature,*
554 **498**, 51-59.

555 Harper, J., Humphrey, N., Pfeffer, W. T., Brown, J. & Fettweis, X. (2012). Greenland ice-sheet
556 contribution to sea-level rise buffered by meltwater storage in firn. *Nature,* **491**, 240-3.

557 Hasholt, B., Mikkelsen, A. B., Nielsen, M. H. & Larsen, M. A. D. (2013). Observations of Runoff
558 and Sediment and Dissolved Loads from the Greenland Ice Sheet at Kangerlussuaq, West
559 Greenland, 2007 to 2010. *Zeitschrift für Geomorphologie,* **57** (Suppl. 2), 3-27.

560 Huggell, C., Kaab, A., Haeberli, W., Teysseire, P. & Paul, F. (2002). Remote sensing based
561 assessment of hazards from glacier lake outbursts: a case study in the Swiss Alps. *Canadian*
562 *Geotechnical Journal,* **39**, 316-330.

563 Humphrey, N. F., Harper, J. T. & Pfeffer, W. T. (2012). Thermal tracking of meltwater retention in
564 Greenland's accumulation area. *Journal of Geophysical Research-Earth Surface,* **117**.

565 Huybrechts, P., Goelzer, H., Janssens, I., Driesschaert, E., Fichefet, T., Goosse, H. & Loutre, M. F.
566 (2011). Response of the Greenland and Antarctic Ice Sheets to Multi-Millennial Greenhouse
567 Warming in the Earth System Model of Intermediate Complexity LOVECLIM. *Surveys in*
568 *Geophysics,* **32**, 397-416.

569 Irvine-Fynn, T. D. L., Hodson, A. J., Moorman, B. J., Vatne, G. & Hubbard, A. L. (2011). Polythermal
570 glacier hydrology: a review. *Reviews of Geophysics,* **49**, RG4002.

571 Krawczynski, M., Behn, M., Das, S., and Joughin, I. (2009). Constraints on the lake volume required
572 for hydro-fracture through ice sheets, *Geophys. Res. Lett.*, 36, 1–5,
573 doi:10.1029/2008GL036765.

574 Keegan, K. M., Albert, M. R., McConnell, J. R. & Baker, I. (2014). Climate change and forest fires
575 synergistically drive widespread melt events of the Greenland Ice Sheet. *Proceedings of the*
576 *National Academy of Sciences of the United States of America,* **111**, 7964-7967.

577 Machguth, H., MacFerrin, M., van As, D., Box, J., E., Charalampidis, C., Colgan, W., Fausto, R., S.,
578 Meijer, H., A., J., Mosley-Thompson, E. and van de Wal, R., S., W. Greenland meltwater
579 storage in firn limited by near-surface ice formation (2016). *Nature Climate Change,* 1-6.

McGrath, D., Colgan, W., Bayou, N., Atsuhiro, M. & Konrad, S. (2013). Recent warming at Summit, Greenland: Global contect and implications. *Geophysical Research Letters,* **40**, 2091-2096.

Mikkelsen, A. B., Hasholt, B., Knudsen, N. T. & Nielsen, K. (2013). Jökulhlaups and sediment transport in Watson River, Kangerlussuaq, West Greenland. *Hydrology Research,* **44**, 58-67.

Neff, W., Compo, G. P., Ralph, F. M. & Shupe, M. D. (2014). Continental heat anomalies and the extreme melting of the Greenland ice surface in 2012 and 1889. *Journal of Geophysical Research-Atmospheres,* **119**, 6520-6536.

Nghiem, S. V., Hall, D. K., Mote, T. L., Tedesco, M., Albert, M. R., Keegan, K., Shuman, C. A., DiGirolamo, N. E. & Neumann, G. (2012). The extreme melt across the Greenland ice sheet in 2012. *Geophysical Research Letters,* **39**, L20502.

Nick, F. M., Luckman, A., Vieli, A., van der Veen, C. J., van As, D., van de Wal, R. S. W., Pattyn, F., Hubbard, A. L. & Floricioiu, D. (2012). The response of Petermann Glacier, Greenland, to large calving events, and its future stability in the context of atmospheric and oceanic warming. *Journal of Glaciology,* **58** (208), 229-239.Pfeffer, W. T., Meier, M. F. & Illangasekare, T. H. (1991). Retention of Greenland Runoff by Refreezing - Implications for Projected Future Sea-Level Change. *Journal of Geophysical Research-Oceans,* **96**, 22117-22124.

Rennermalm, A., Moustafa, S., Mioduszewski, J., Chu, V., Forster, R., Hagedorn, B., Harper, J., Mote, T., Robinson, D., Shuman, C. & others (2013). Understanding Greenland ice sheet hydrology using an integrated multi-scale approach. *Environmental Research Letters,* **8**, 015017.

Russell, A. J., Carrivick, J. L., Ingeman-Nielsen, T., Yde, J. C. & Williams, M. (2011). A new cycle of jokulhlaups at Russell Glacier, Kangerlussuaq, West Greenland. *Journal of Glaciology,* **57**, 238-246.

Selmes, N., Murray, T. & James, T. D. (2011). Fast draining lakes on the Greenland Ice Sheet. *Geophysical Research Letters,* **38**, L15501.

Smith, L. C., Chu, V. W., Yang, K., Gleason, C. J., Pitcher, L. H., Rennermalm, A. K., Legleiter, C. J., Behar, A. E., Overstreet, B. T., Moustafa, S. E., Tedesco, M., Forster, R. R., LeWinter, A. L., Finnegan, D. C., Sheng, Y. & Balog, J. (2015). Efficient meltwater drainage through supraglacial streams and rivers on the southwest Greenland ice sheet. *Proceedings of the National Academy of Sciences,* **112**, 1001-1006.

Tedesco, M., Fettweis, X., Mote, T., Wahr, J., Alexander, P., Box, J. E. & Wouters, B. (2013). Evidence and analysis of 2012 Greenland records from spaceborne observations, a regional climate model and reanalysis data. *The Cryosphere,* **7**, 615-630.

Tedesco, M., Fettweis, X., van den Broeke, M. R., van de Wal, R. S. W., Smeets, C. J. P. P., van de Berg, W. J., Serreze, M. C. & Box, J. E. (2011). The role of albedo and accumulation in the 2010 melting record in Greenland. *Environmental Research Letters,* **6**, 1-6.

van As, D., Hubbard, A. L., Hasholt, B., Mikkelsen, A. B., van den Broeke, M. R. & Fausto, R. S. (2012). Large surface meltwater discharge from the Kangerlussuaq sector of the Greenland ice sheet during the record-warm year 2010 explained by detailed energy balance observations. *The Cryosphere,* **6**, 199-209.

van de Wal, R. S. W., Boot, W., Smeets, C. J. P. P., Snellen, H., van den Broeke, M. R. & Oerlemans, J. (2012). Twenty-one years of mass balance observations along the K-transect, West Greenland. *Earth System Science Data,* **4**, 31-35.

van de Wal, R. S. W., Greurell, W., van den Broeke, M. R., Reijmer, C. H. & Oerlemans, J. (2005). Surface mass-balance observations and automatic weather station data along a transect near Kangerlussuaq, West Greenland. *Annals of Glaciology,* **42 %6**, 311-316 %&.

van de Wal, R. S. W., Smeets, C. J. P. P., Boot, W., Stoffelen, M., van Kampen, R., Doyle, S. H., Wilhelms, F., van den Broeke, M. R., Reijmer, C. H., Oerlemans, J. & Hubbard, A. (2015). Self-regulation of ice flow varies across the ablation area in south-west Greenland. *The Cryosphere,* **9**, 603-611.

van den Broeke, M., Smeets, P., Ettema, J. & Munneke, P. K. (2008). Surface radiation balance in the ablation zone of the west Greenland ice sheet. *Journal of Geophysical Research,* **113**, D13105.

Wientjes, I. G. M., De Van Wal, R. S. W., Schwikowski, M., Zapf, A., Fahrni, S. & Wacker, L. (2012). Carbonaceous particles reveal that Late Holocene dust causes the dark region in the western ablation zone of the Greenland ice sheet. *Journal of Glaciology,* **58**, 787-794.

Wientjes, I. G. M. & Oerlemans, J. (2010). An explanation for the dark region in the western melt zone of the Greenland ice sheet. *The Cryosphere,* **4**, 261-268.

641 **Table 1:** Energy inputs in 2010 and 2012 (TW).

Energy inputs - 0 to 1850 m.a.sl.

	2010	2012	2012-2010
Energy available for melt	2.43×10^6	2.37×10^6	-3 %

642
643
644
645 **Table 2:** Melt contributions (km^3) from different elevation intervals integrated through end of melt
646 season, 1 Oct each year

	2010	**2012**	**Difference**
	km^3	km^3	%
Below mean ELA	6.8	6.3	-7
1550 to 1850 m	0.4	0.7	97
1850 to 2050 m	0.1	0.3	232
Total - up to 1850 m	7.1	7.0	-2
Total - up to 2050 m	7.2	7.3	1
% melt above mean ELA (1550 to 1850 m)	5.6 (%)	10.0 (%)	78
Measured proglacial discharge at Oct. 1	5.3	6.8	28
Integrated melt up 1850 m – measured discharge	1.8	0.2	-90
Integrated melt up 2050 m – measured discharge	1.9	0.5	-74

647

Figures

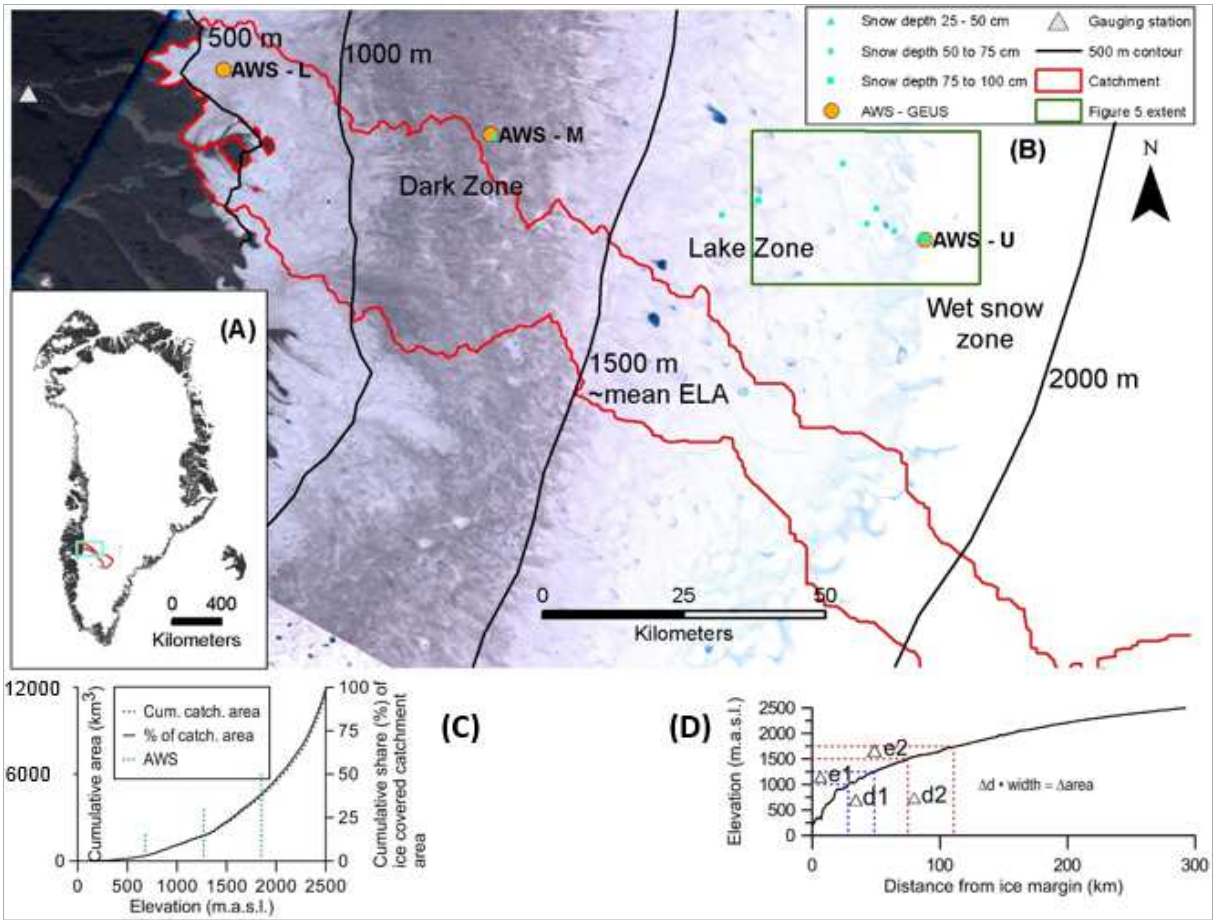

Figure 1: (A) The location of the study area (cyan) and catchment (red) in Greenland is shown on the inset map. (B) Map of the study area overlain with the location of the AWS, gauging station, catchment area, and snow pit sites. The background Landsat 7 image, which was acquired on 16 July 2012, reveals surface water in lakes and streams occurred at an exceptional and unprecedented elevation of ~ 1840 m asl. The non-linear increase in the size of the catchment with increasing elevation is shown in (C) and (D) shows an example of the impact on melt area with a rise in the snow line of 250 m with a 500 m displacement in different start elevations (hypsometric effect).

Figure 2: Photograph taken at 18:00 West Greenland Summer Time on 11 July 2012 during the flood with the Watson River bridge being washed-out. Courtesy of Jens Christiansson.

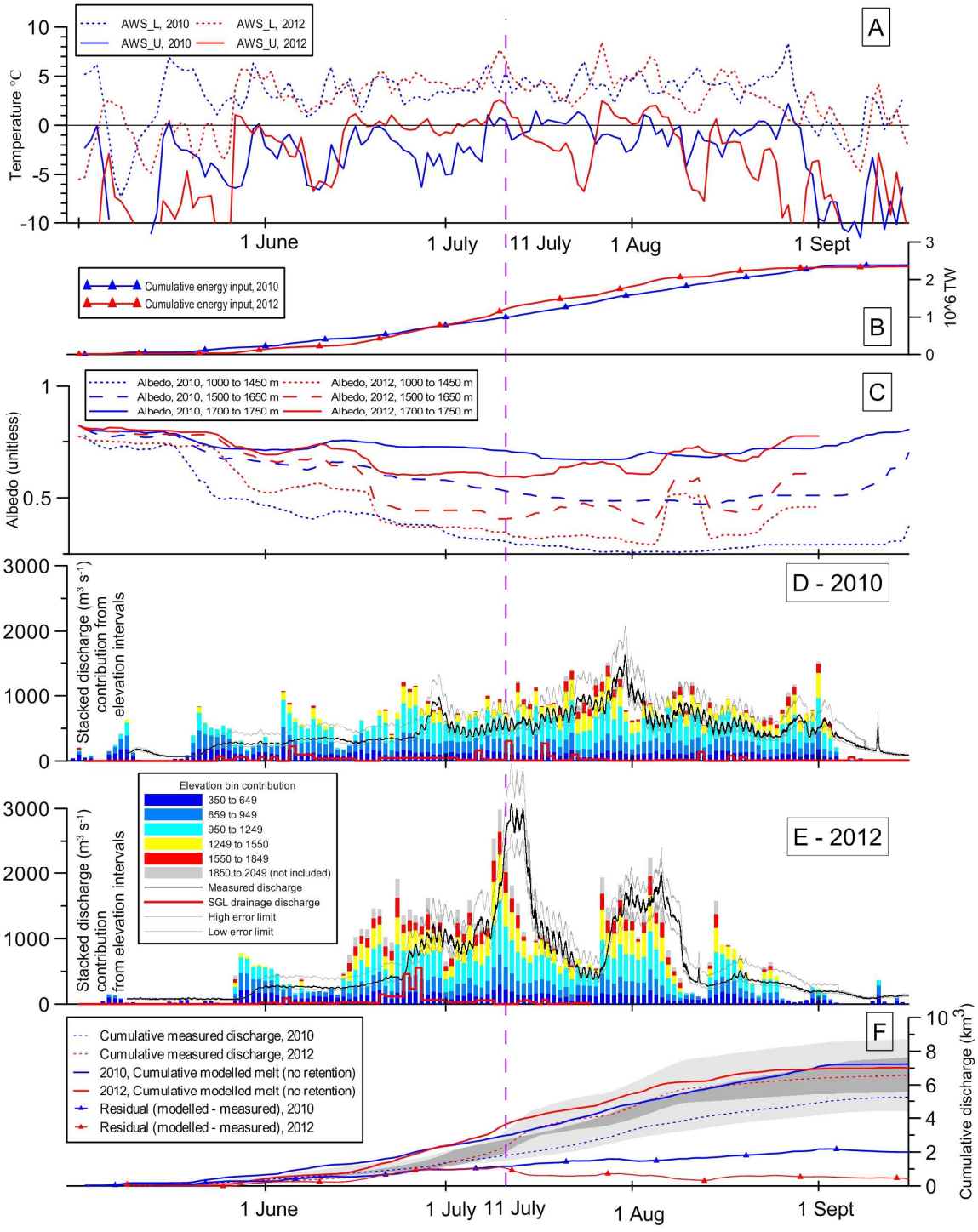
A
AWS_L, 2010
AWS_L, 2012
AWS_U, 2010
AWS_U, 2012
Temperature °C
10
5
0
-5
-10
1 June
1 July
11 July
1 Aug
1 Sept
B
Cumulative energy input, 2010
Cumulative energy input, 2012
10^6 TW
3
2
1
0
C
Albedo, 2010, 1000 to 1450 m
Albedo, 2010, 1500 to 1650 m
Albedo, 2010, 1700 to 1750 m
Albedo, 2012, 1000 to 1450 m
Albedo, 2012, 1500 to 1650 m
Albedo, 2012, 1700 to 1750 m
Albedo (unitless)
1
0.5
D - 2010
Stacked discharge (m³ s⁻¹) contribution from elevation intervals
3000
2000
1000
0
E - 2012
Elevation bin contribution
350 to 649
659 to 949
950 to 1249
1249 to 1550
1550 to 1849
1850 to 2049 (not included)
Measured discharge
SGL drainage discharge
High error limit
Low error limit
F
Cumulative measured discharge, 2010
Cumulative measured discharge, 2012
2010, Cumulative modelled melt (no retention)
2012, Cumulative modelled melt (no retention)
Residual (modelled - measured), 2010
Residual (modelled - measured), 2012
Cumulative discharge (km³)
10
8
6
4
2
0

661

Figure 3: Meteorological records, discharge measurements and modelled melt runoff for the study area during 2010 and 2012, including **(A)** daily average air temperature at AWS_L and AWS_U. (To avoid cluttering the plot the air temperature at AWS_U is only plotted during summer and the air temperature at AWS_M , which usually les between that of AWS_L and AWS_U is not plotted at all). **(B)** the calculated cumulative energy input, **(C)** the albedo at three different elevation bands, **(D, E)** the proglacial discharge, supraglacial lake drainage volume, and modelled melt runoff, and **(F)** the cumulative proglacial discharge, modelled melt runoff, and residual between the two. The dashed vertical purple line demarks the bridge wash out on 11 July 2012. The uncertainty in discharge estimates is shown using grey lines on (d) and (e) and by grey shading on (f). Where the uncertainty estimates for 2010 and 2012 overlap on (f) a darker shade of grey is used.

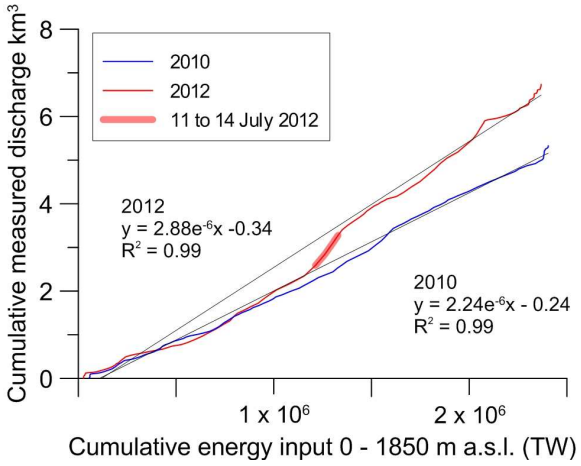

Figure 4: The cumulative measured discharge as a function of the calculated energy input for the catchment up to 1850 m a.s.l. The flooding period of 11 to 14 July is marked with a bold red line.

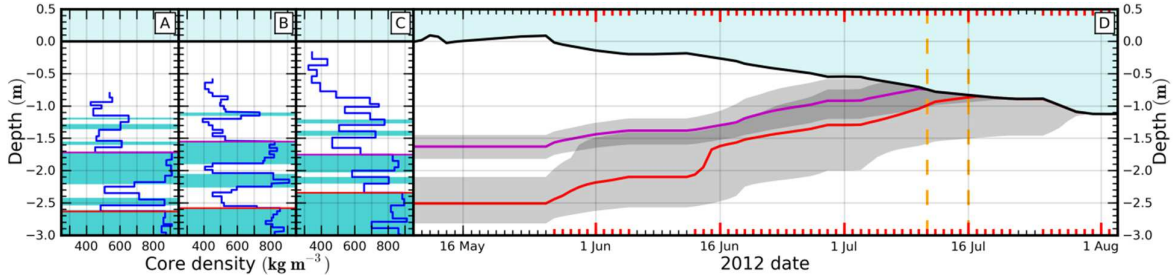

Figure 5: (A-C) Density profiles of three shallow firn cores (A-C respectively) drilled at AWS_U in May 2012. The water table is indicated in light blue and ice lenses observed in the core straigraphy are indicated in cyan. Magenta and red lines indicate two potential sets of "blocking" ice lenses

observed in the firn. (D) A model simulation of the near-surface water table at AWS_U for each of the two blocking lens assumptions in A-C, with 95% confidence intervals in grey. Red ticks on the horizontal axes indicate days above freezing when surface melt would occur. As snow melts above the blocking lenses the water table rises simultaneously until it meets the lowering snow surface. Light blue is free air. The daily snow surface is observed by the adjacent AWS_U AWS. The two dashed orange vertical lines indicate 11 July, the date of the Watson River bridge destruction, and 16 July, when the Landsat image from Figure 1 shows horizontal water transport in the vicinity of AWS_U.

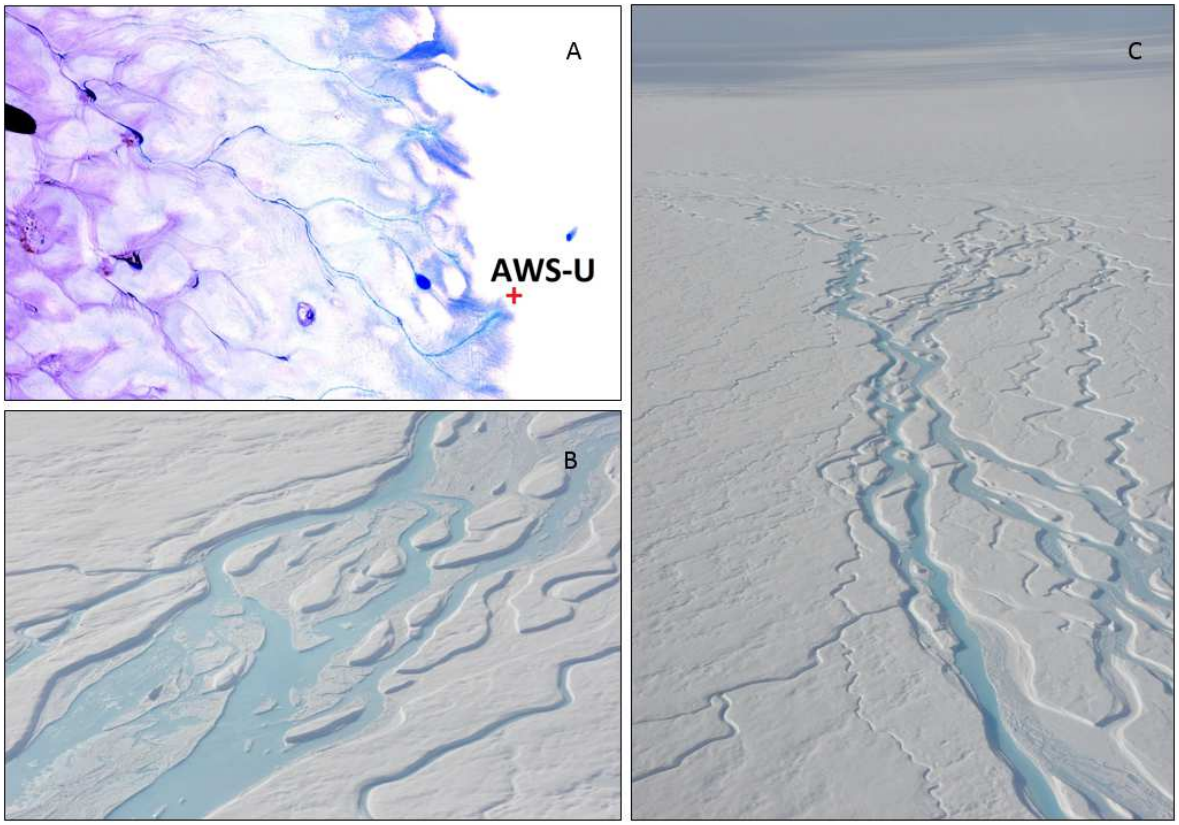

Figure 6: (A) Zoom in on Landsat 7 image from 16 July 2012 showing free surface water in the area around AWS_U. The extent is marked on Figure 1. The scan line correction failure was interpolated using the ENVI 'replace bad data' routine based on Band 8 and visible surface water was enhanced using a modified normalized difference water index (Fitzpatrick et al., 2014). (B and C) Oblique aerial photographs of the active surpraglacial channel netowk emerging from AWS_U well within

the accumulation zone at 1840 m a.s.l. and 140 km from the ice sheet margin on 13 August 2012. Courtesy of Paul Smeets.